

Self-consistent multidimensional Penrose process driven by magnetic reconnection

Filippo Camilloni¹ and Luciano Rezzolla^{1,2,3}

¹*Institut für Theoretische Physik, Goethe Universität, Max-von-Laue-Str. 1, 60438 Frankfurt am Main, Germany*

²*Frankfurt Institute for Advanced Studies, Ruth-Moufang-Str. 1, 60438 Frankfurt am Main, Germany*

³*School of Mathematics, Trinity College, Dublin 2, Ireland*

(Dated: November 8, 2024)

Astronomical observations and numerical simulations are providing increasing evidence that resistive effects in plasmas around black holes play an important role in determining the phenomenology observed from these objects. In this spirit, we present a general approach to the study of a Penrose process driven by plasmoids that are produced at reconnection sites along current sheets. Our formalism is meant to determine the physical conditions that make a plasmoid-driven Penrose process energetically viable and can be applied to scenarios that are matter- or magnetic-field-dominated, that is, in magnetohydrodynamical or force-free descriptions. Our approach is genuinely multidimensional and hence allows one to explore conditions that are beyond the ones explored so far and that have been restricted to the equatorial plane, thus providing a direct contact with numerical simulations exhibiting an intense reconnection activity outside the equatorial plane. Finally, our analysis does not resort to ad-hoc assumptions about the dynamics of the plasma or adopts oversimplified and possibly unrealistic models to describe the kinematics of the plasma. On the contrary, we study the dynamics of the plasma starting from a well-known configuration, that of an equilibrium torus with a purely toroidal magnetic field whose “ergobelt”, i.e., the portion penetrating the ergosphere, naturally provides a site to compute, self-consistently, the occurrence of reconnection and estimate the energetics of a plasmoid-driven Penrose process.

Introduction. In a resistive plasma, magnetic reconnection consists in a sudden rearrangement of the magnetic-field topology caused by the local interaction of field lines with opposite polarity. This process leads to a rapid conversion of magnetic energy into thermal and kinetic energy of two plasma outflows with locally isotropic properties and moving in opposite directions at relativistic speeds, the plasmoids. The ubiquitous and fundamental role played by magnetic reconnection in astrophysical plasmas is now widely recognized on scales ranging from stellar flares and coronal mass ejections [1–3], to high-energy sources such as pulsar magnetospheres [4], accreting black holes (BHs) [5–8], and binary neutron-star mergers leading to the short gamma-ray burst phenomenology [9–15].

Recent numerical simulations, either in magnetohydrodynamics (MHD) or with particle-in-cell (PIC) approaches, have unfolded a rich phenomenology associated to magnetic reconnection and plasmoid generation, thus enhancing our understanding of these processes both in special-relativistic regimes [16–22], and when general-relativistic effects become relevant [23–27]. In this regard, astrophysical BHs constitute unique theoretical laboratories to explore extreme conditions of plasma electrodynamics. Indeed, one of the most remarkable predictions of general relativity is the possibility of extracting rotational energy of the BH by invoking the negative inflow of energy and angular momentum at the horizon [28], with various processes differing only in the physical agent operating the extraction. Notorious examples range from single particles associated to mechanical [29] and collisional Penrose process (PP) [30–33], to super-radiant scalar fields [34–37], and to force-free electrodynamics (FFE) fields in the Blandford–Znajek (BZ) mechanism [38].

Given the presence of strong magnetic fields and relativistic plasmas near astrophysical BHs, it is natural to expect a manifestation of the PP triggered by magnetic reconnection and

mediated by plasmoids. This idea was originally proposed and explored analytically by Koide and Arai [23], to be further reviewed and extended by Asenjo and Comisso [24, 26], who computed the power extracted and the efficiency of the process in terms of the local reconnection rate (see also [25] for related PIC simulations). Despite the importance of these initial works, they contain a number of approximations that prevent from testing them in numerical environments and assessing their viability in realistic astrophysical scenarios. Arguably, the most serious of these limitations rests with the lack of a self-consistent description of the plasma dynamics, either in the MHD or FFE regimes. In turn, this forces the use of number of assumptions on the dynamics of the plasma that are either far from known solutions and numerical simulations (see, e.g., [39–45]), or difficult to realise in practice.

To overcome these difficulties, it is important to construct reconnection models that are consistent with well-known plasma solutions or that share dynamical features and conditions that are similar to those encountered in simulations. In this Letter, we address these issues by exploiting a self-consistent, fully covariant analytic description of plasma and fields of degenerate electrodynamics that includes ideal MHD and FFE as particular examples. More specifically, we analyse for the first time the conditions under which a distribution of magnetised matter penetrating the ergosphere and not restricted to the equatorial plane can produce plasmoids with negative energy-at-infinity. In this way, we can study the extraction of energy and angular momentum from a Kerr BH in a self-consistent scenario that is not too far from the conditions explored in simulations.

Degenerate electrodynamics around a Kerr BH. We consider the electrodynamics of a Kerr BH with mass M and specific angular momentum a . In a 3+1 decomposition, the metric can be written in terms the lapse function α , the shift vector β^ϕ and the spatial metric γ_{ij} [46] (see End Mat-

ter). Both the electromagnetic and the matter properties inherit constraints from the requirements that the electromagnetic fields are *degenerate*, i.e., $\eta_{\mu\nu\rho\sigma}F^{\mu\nu}F^{\rho\sigma} = 0$, and magnetically-dominated, i.e., $F_{\mu\nu}F^{\mu\nu} > 0$ [47] (F is the Faraday tensor with dual $*F$ and $\eta_{\mu\nu\rho\sigma}$ the Levi-Civita symbol). These covariant conditions enforce the orthogonality of electric and magnetic fields and are violated only on the microscopical scales of the current-sheets where reconnection takes place [16]. Degeneracy also implies that stationary and axisymmetric fields are expressed in terms of the magnetic-flux function $\Psi = \Psi(r, \theta)$, determining the poloidal magnetic fields, the poloidal current $I = I(r, \theta)$ (which is proportional to the toroidal field), and the angular velocity of the magnetic-field lines $\Omega = \Omega(\Psi)$ [47].

A particularly convenient class of observers is that with Zero Angular Momentum (ZAMOs) with worldline tangent $\eta := \eta^\mu \partial_\mu = \alpha^{-1}(\partial_t + \omega_z \partial_\phi)$, and whose angular velocity is $\omega_z := -\beta^\phi$. Such an observer carries a local orthonormal (Cartesian) tetrad, $\hat{e}_{(\alpha)}$ with $\alpha = T, X, Y, Z$, such that on the equatorial plane ($\theta = \pi/2$), the X and Y legs align respectively with the r and ϕ directions, whereas the Z leg is orthogonal to the equatorial plane and parallel to the BH spin (quantities in the ZAMO frame are marked with a “hat” and the components with bracketed indices).

The magnetic field in the ZAMO frame is purely spatial, $\hat{\mathbf{B}} = \hat{B}^{(\alpha)} \hat{e}_{(\alpha)} = (\partial_\theta \Psi / \sqrt{\Pi} \sin \theta) \hat{e}_{(X)} - (I / \sqrt{\Delta} \sin \theta) \hat{e}_{(Y)} + (\sqrt{\Delta} \partial_r \Psi / \sqrt{\Pi} \sin \theta) \hat{e}_{(Z)}$, while the electric field is orthogonal to $\hat{\mathbf{B}}$ and has components $\hat{\mathbf{E}} = \hat{E}^{(\alpha)} \hat{e}_{(\alpha)} = \sqrt{\gamma_{\phi\phi}} / \alpha (\omega_z - \Omega) (\hat{B}^{(Z)} \hat{e}_{(X)} - \hat{B}^{(X)} \hat{e}_{(Z)})$. The orthogonality of the electric and magnetic fields to each other and to the ZAMO four-velocity implies the following set of orthonormal vectors [48, 49]

$$\begin{aligned} \mathcal{T}^{(\alpha)} &:= \eta^{(\alpha)}, & \mathcal{X}^{(\alpha)} &:= \frac{\hat{E}^{(\alpha)}}{\sqrt{\mathcal{E}^2}}, & \mathcal{Y}^{(\alpha)} &:= \frac{\hat{B}^{(\alpha)}}{\sqrt{\mathcal{B}^2}}, \\ \mathcal{Z}^{(\alpha)} &:= \epsilon^{(\alpha)(\beta)(\gamma)(\delta)} \mathcal{T}_{(\beta)} \mathcal{X}_{(\gamma)} \mathcal{Y}_{(\delta)}. \end{aligned} \quad (1)$$

The plasma four-velocity as measured by a ZAMO admits the generic decomposition $\hat{\mathbf{u}} = \hat{u}^{(\alpha)} \hat{e}_{(\alpha)} = \hat{\gamma}(\mathcal{T} + \hat{v}_\parallel \mathcal{Y} + \hat{v}_\perp \mathcal{Z})$ [48–51], where the \parallel and \perp symbols mark the orientation with respect to the magnetic-field lines. Such a decomposition has the advantage that the spatial velocity orthogonal to the fields is solely specified by the electromagnetic sector, $\hat{v}_\perp := \mathcal{E}/\mathcal{B}$, and the corresponding Lorentz factor is $\hat{\gamma}_\perp := \sqrt{\mathcal{B}^2/(\mathcal{B}^2 - \mathcal{E}^2)}$, where $\mathcal{B}^2 - \mathcal{E}^2 > 0$. The total Lorentz factor $\hat{\gamma}$ is given by $\hat{\gamma} := 1/\sqrt{1 - \hat{v}_\perp^2 - \hat{v}_\parallel^2}$, and we note that flows with $\hat{\gamma} = \hat{\gamma}_\perp$ (i.e., with $\hat{v}_\parallel = 0$) provide a unique covariant definition of timelike observers in FFE characterised by $\vec{E} \times \vec{B}$ drift velocities [48]. Since the total Lorentz factor can also be expressed as $\hat{\gamma}^2 = \hat{\gamma}_\perp^2 / (1 - \hat{\gamma}_\perp^2 \hat{v}_\parallel^2)$, it follows that $\hat{\gamma} \geq \hat{\gamma}_\perp$, namely, $\hat{\gamma} = \hat{\gamma}_\perp$ for $\hat{v}_\parallel = 0 =: \hat{v}_\parallel^{\min}$, and

$\hat{\gamma} \rightarrow \infty$ for $\hat{v}_\parallel = \hat{\gamma}_\perp^{-1} =: \hat{v}_\parallel^{\max}$ [49].

Because reconnection is normally studied locally, i.e., in the frame comoving with the plasma [16], we introduce the comoving frame with timelike tangent given by the plasma four-velocity \mathbf{u} . In the ideal-MHD limit of infinite electrical conductivity, any electric field is zero in the frame comoving with the fluid, so that if we define the electric, \mathbf{e} , and magnetic, \mathbf{b} , fields in the comoving frame respectively as $e^\mu := F^{\mu\nu} u_\nu$ and $b^\mu := *F^{\mu\nu} u_\nu$, then $e^\mu = 0$ by construction. Note that while we will employ a comoving frame to compute the details of the reconnection and plasmoid production, we will always make use of the electromagnetic fields in the ZAMO frame, $\hat{\mathbf{E}}$ and $\hat{\mathbf{B}}$, so that the comoving magnetic field is $\mathbf{b} := [\hat{\mathbf{B}} + (\hat{\mathbf{u}} \cdot \hat{\mathbf{B}}) \hat{\mathbf{u}}] / \hat{\gamma}$ and $b^2 := \mathbf{b} \cdot \mathbf{b} = \mathcal{B}^2 - \mathcal{E}^2$.

In the frame comoving with the fluid, we assume that two plasmoids are ejected locally tangent to the current-sheet with opposite “outflow” velocities $\pm \tilde{v}_{\text{out}}$, where the signs distinguish the plasmoid ejected in the direction parallel (+) or antiparallel (−) to the magnetic-field lines. The initial outflow four-velocity of the plasmoids is thus $\tilde{\mathbf{u}}_{\text{out}} = \tilde{\gamma}_{\text{out}}(\hat{\mathbf{u}} \pm \tilde{v}_{\text{out}} \mathbf{b}/b)$, with the azimuthal velocity and Lorentz factor measured by the ZAMO given by

$$\begin{aligned} \hat{v}_{\text{out}}^{(Y)} &= \frac{(\hat{\gamma}_\perp \hat{v}_\parallel \pm \tilde{v}_{\text{out}}) \hat{B}^{(Y)}}{\hat{\gamma}_\perp (1 \pm \hat{\gamma}_\perp \hat{v}_\parallel \tilde{v}_{\text{out}}) \mathcal{B}} - \hat{v}_\perp \frac{\sqrt{\hat{B}_{(X)}^2 + \hat{B}_{(Z)}^2}}{\mathcal{B}}, \\ \hat{\gamma}_{\text{out}} &= \hat{\gamma} \tilde{\gamma}_{\text{out}} (1 \pm \hat{\gamma}_\perp \hat{v}_\parallel \tilde{v}_{\text{out}}). \end{aligned} \quad (2)$$

Plasmoids, RAIBs, and PP. To define the details of the PP we need a local model for magnetic reconnection that provides a prescription for the velocity field \tilde{v}_{out} of the plasmoids and their energetics. Such a model will have to account for the redistribution of the magnetic energy into the kinetic and internal energy of the plasmoid. The details of this conversion can be extremely difficult to calculate under realistic conditions and probably require a microscopical description involving PIC simulations [21, 22]. However, to make some analytic progress, we use the so-called Relativistic Adiabatic Incompressible Ball (RAIB) model [23], normally adopted under these conditions (see Refs. [24, 26] and related works). Notwithstanding some of their limitations, RAIBs represent the simplest but non-trivial model of plasmoids, which are treated as localised distributions of energy dressed with an additional pressure term that contributes to their inertia and is reminiscent of their hydrodynamical nature. The RAIB energy-at-infinity needed to estimate the extraction of energy from a reconnection-driven PP follows upon integrating the energy-momentum tensor of a perfect fluid and reads [23]

$$E^\infty = \alpha H \left[\hat{\gamma}_{\text{out}} \left(1 + \frac{\sqrt{\gamma_{\phi\phi}}}{\alpha} \omega_z \hat{v}_{\text{out}}^{(Y)} \right) - \frac{U(\Gamma - 1)}{H \hat{\gamma}_{\text{out}}} \right], \quad (3)$$

with H , U , and Γ the total enthalpy, internal energy and adiabatic index in the plasmoid, respectively. Hence, the energy-at-infinity per unit enthalpy, $\epsilon^\infty := E^\infty/H$, is

$$\varepsilon_{\pm}^{\infty} = \alpha \hat{\gamma} \left[\left(1 + \left(\hat{v}_{\parallel} \frac{\hat{\mathcal{B}}^{(Y)}}{\mathcal{B}} - \hat{v}_{\perp} \frac{\sqrt{\hat{\mathcal{B}}_{(X)}^2 + \hat{\mathcal{B}}_{(Z)}^2}}{\mathcal{B}} \right) \frac{\sqrt{\gamma_{\phi\phi}} \omega_z}{\alpha} \right) \tilde{\gamma}_{\text{out}} + \right. \\ \left. \pm \left(\hat{v}_{\parallel} \hat{\gamma}_{\perp} + \left(\frac{\hat{\mathcal{B}}^{(Y)}}{\hat{\gamma}_{\perp} \mathcal{B}} - \hat{v}_{\parallel} \hat{v}_{\perp} \hat{\gamma}_{\perp} \frac{\sqrt{\hat{\mathcal{B}}_{(X)}^2 + \hat{\mathcal{B}}_{(Z)}^2}}{\mathcal{B}} \right) \frac{\sqrt{\gamma_{\phi\phi}} \omega_z}{\alpha} \right) \tilde{v}_{\text{out}} \tilde{\gamma}_{\text{out}} - \frac{U(\Gamma - 1)/H}{\hat{\gamma}^2 \tilde{\gamma}_{\text{out}} (1 \pm \hat{\gamma}_{\perp} \hat{v}_{\parallel} \tilde{v}_{\text{out}})} \right]. \quad (4)$$

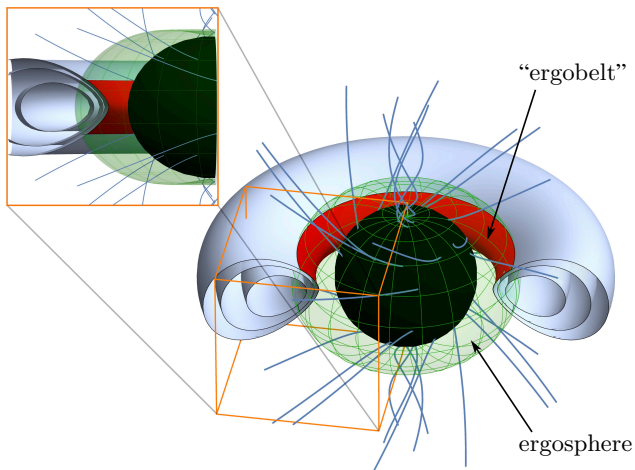


FIG. 1. Shown with grey contours are the iso-levels of the rest-mass density of a torus with a toroidal magnetic field entering the BH ergosphere (green region). Reconnection and plasmoid production can take place on the surface of the torus and if this happens in the ergoregion, i.e., on the “ergobelt” (red region), then a PP can be activated from plasmoids having a negative energy-at-infinity.

Expression (4) contains information not only on the background geometry via the metric functions α , ω_z , and $\gamma_{\phi\phi}$, but also on the global magnetic-field configuration around the BH, either via the magnetic field components $\hat{\mathcal{B}}^{(\alpha)}$, or through the field strength given by $\hat{v}_{\perp} = \mathcal{E}/\mathcal{B}$. In addition, the dynamics of the bulk plasma is encoded in \hat{v}_{\parallel} , that should be prescribed together with the coordinate invariant quantities $\Psi(r, \theta)$, $I(r, \theta)$, and $\Omega(\Psi)$. Note that Eq. (4) is consistent with any stationary and axisymmetric solution in ideal MHD and in FFE, and can be used to model BH-energy extraction by plasmoids in more realistic configurations. By contrast, previous models were restricted to the equatorial plane and invoked a Keplerian dynamics not realistic within the ergosphere [23, 24, 26].

Magnetised torus. To achieve a self-consistent treatment of reconnection outside the equatorial plane, we apply our general treatment to a Komissarov’s torus with a toroidal magnetic field corotating with the BH [52–54]¹. The presence of

the inner light surface will inevitably lead to toroidal magnetic fields in the ergoregion that are dominant and oriented in the counterrotating direction [47, 50, 55–57]. Under these conditions, the torus surface will develop a current-sheet and act as an optimal site for the production plasmoids. Furthermore, the portion of the torus surface that is inside the ergosphere and undergoes reconnection, i.e., what we dub “*ergobelt*” (red region in Fig. 1), can generate plasmoids that have negative energy-at-infinity and hence tap the BH rotational energy via a plasmoid-driven PP. Note that the current sheet on the torus surface will also be accompanied by the standard equatorial current-sheet that inevitably develops for split-field configurations; we refer to [23–26, 47, 57] to review the phenomenology and energetics associated to these current sheets.

Such a magnetised torus provides us a non-trivial configuration that is mathematically self-consistent and does not invoke unrealistic assumptions. Indeed, numerical simulations either in MHD [39–43, 45] or with PIC approaches [58–60] have shown that the accretion disc around a supermassive BH develops a toroidal component and that the transition region between the torus and the funnel systematically leads to reconnection phenomena. The Komissarov solution naturally entails that $\Psi = 0$ and $\hat{v}_{\parallel} = \ell_0 \alpha / [\sqrt{\gamma_{\phi\phi}} (\omega_z \ell_0 - 1)]$, so that $\hat{v}_{\perp} = 0$ and $\hat{\mathcal{B}}^{(X)} = \hat{\mathcal{B}}^{(Z)} = 0$ (see End Matter). Hereafter we will consider maximally-filled tori with $\ell_0 \approx \ell_{\text{mb}}$ and $\mathcal{W}_{\text{in}} = \mathcal{W}_{\text{cusp}} = 0$.

Following [23, 26], we assume the plasmoids/RAIBs to consist of relativistically-hot plasma described by an ideal-fluid equation of state so that $H = 4U(\Gamma - 1)$. Moreover, we use the analytic model of magnetic reconnection in Ref. [16] predicting plasmoid velocities that are simple functions of the magnetisation $\sigma_0 := b^2/w_0$, where w_0 is the enthalpy density. More specifically, we set $\tilde{v}_{\text{out}} \approx \sqrt{\sigma_0/(1 + \sigma_0)}$ and $\tilde{\gamma}_{\text{out}} \approx \sqrt{1 + \sigma_0}$ [61], so that Eq. (4) simplifies and becomes dependent on the BH spin a , the plasma magnetisation σ_0 ², the torus angular momentum ℓ_0 , and the (r, θ) location of the ergobelt [see Eq. (13) in End Matter].

¹ Under realistic conditions of accretion, the magnetic field will also will have a poloidal component in the torus and in the jet, which however does not participate in the reconnection we discuss here, which only requires a toroidal component.

² Typical magnetisation just inside the torus is $\sim \mathcal{O}(0.01 - 0.1)$ with vanishing magnetic fields at the surface. Numerical simulations show that σ_0 jumps to $\sim \mathcal{O}(10 - 100)$ just outside the torus [39–43, 45]. Hence, to model the reconnection in the transition region in the vicinity of the ergobelt we consider $0.1 \lesssim \sigma_0 \lesssim 10$.

¹ Under realistic conditions of accretion, the magnetic field will also will have a poloidal component in the torus and in the jet, which however does

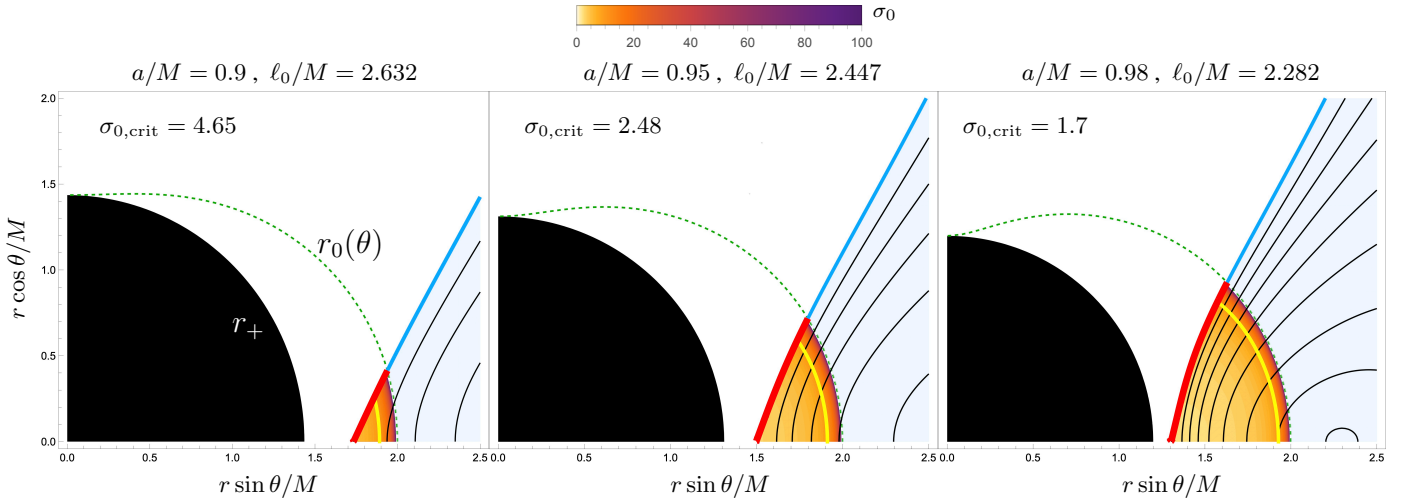


FIG. 2. Polar sections of tori with $\ell_0 \simeq \ell_{\text{mb}}$ (light blue shading) entering the ergosphere r_0 (green dashed line), with BH spin increasing from left to right. The torus surface inside the ergosphere, dubbed ergobelt (red solid line), is suitable for reconnection to drive a PP. The colormap reports values of the magnetisation σ_0 necessary for the pair-production of plasmoids with $\varepsilon_+^\infty > 0$ and $\varepsilon_-^\infty < 0$ at different positions in the torus, with the yellow solid line marking $\sigma_0 = 10$.

A number of important remarks should be made on ε_\pm^∞ as obtained above. First, the value at the horizon, $\varepsilon_\pm^\infty|_{r_+}$, is finite for all BH spins. Second, since the conditions for a successful PP require $\varepsilon_+^\infty > 0$ and $\varepsilon_-^\infty < 0$ [26], a critical magnetisation $\sigma_{0,\text{crit}}$ exists that depends on the BH spin and torus properties and below which no PP can take place. For instance, for $a/M = 0.9$ and $\ell_0/M \lesssim 2.63$, $\sigma_{0,\text{crit}} \approx 4.65$, well within what encountered in simulations [41, 42]. Third, in regions where $\sigma_0 \gg 1$, Eq. (4) further simplifies to $\varepsilon_\pm^\infty = \sqrt{\sigma_0} (1 \pm \omega_z \sqrt{\gamma_{\phi\phi}}/\alpha) \sqrt{1 \pm \hat{v}_\parallel}/\sqrt{1 \mp \hat{v}_\parallel}$, showing that plasmoids with $\varepsilon_-^\infty < 0$ can be produced for sufficiently high magnetisation, provided that a portion of the torus intersects the ergosphere where $\omega_z \sqrt{\gamma_{\phi\phi}} \geq \alpha$. For maximally filled tori, the torus cusp is inside the ergosphere if $a > a_{\text{crit}} := 2(\sqrt{2} - 1)M \approx 0.83M$. Finally, and most importantly, because Eq. (4) applied to a torus is not restricted to the equatorial plane, it allows us to study for the first time the problem plasmoid-driven PP in an axisymmetric but non-equatorial context.

Figure 2 shows polar sections of magnetised tori with $\ell_0 \lesssim \ell_{\text{mb}}$ entering the ergosphere of BHs with spin increasing from left to right. Marked with a colormap are the values of the magnetisation σ_0 such that $\varepsilon_+^\infty > 0$ and $\varepsilon_-^\infty < 0$ [cf., Eq. (4)] and reported are corresponding the critical value for the magnetisation. For magnetisations above a critical value $\sigma_{0,\text{crit}}$, the innermost part of the torus possesses an ergobelt as a site for the production of plasmoids with negative energy-at-infinity and hence yield a PP. Moreover, for faster spinning BHs, larger portions of the torus penetrate the ergosphere increasing the potential production of plasmoids.

Energetics of the plasmoid-driven PP. Because of the nonlinear nature of reconnection and of the plasma dynamics near the torus surface, the energy extraction process will be in-

trinsically stochastic, so that the energy-extraction rate \dot{E}_{rec} will depend on the local reconnection rate, routinely assumed to be $\mathcal{R}_{\text{rec}} \simeq 0.1$ [16, 24, 26, 62, 63]. Taking now \mathcal{L} and \mathcal{A} respectively as the linear size and surface area of the ergobelt (note there are two ergobelts, symmetric with respect to the equatorial plane), we approximate the enthalpy density as $w_0 \approx H/(\mathcal{L}\mathcal{A})$ and express the energy extraction rate as $\dot{E}_{\text{rec}} = -2\mathcal{R}_{\text{rec}}w_0 \int_{\mathcal{A}} \varepsilon_-^\infty d\mathcal{A} = -2\mathcal{R}_{\text{rec}}w_0 \mathcal{A} \langle \varepsilon_-^\infty \rangle$, where $\langle \varepsilon_-^\infty \rangle := \int_{\mathcal{A}} \varepsilon_-^\infty d\mathcal{A} / \int_{\mathcal{A}} d\mathcal{A}$ is the energy-at-infinity averaged over the area of the ergobelt (see End Matter).

In the top part of Fig. 3 we report the behaviour of \dot{E}_{rec}/w_0 as a function of the plasma magnetisation and BH spin. As expected, no energy extraction occurs if the BH is not spinning sufficiently fast (the torus does not enter the ergosphere) or if the magnetisation is below the corresponding critical value (red solid line). Conversely, the process is more efficient for rapidly spinning BHs and high magnetisations, since the effective area of the ergobelt then increases. The values of \dot{E}_{rec} are comparable or larger than those estimated in Ref. [26] for plasmoids generated in the equatorial plane.

Finally, we can compare the extracted energy via plasmoids with the power extracted via the BZ mechanism, which, we recall, is steady and effective for any nonzero value of the BH spin. The BZ power extracted by a split-monopole field in Kerr can be written as an expansion in the BH angular velocity, $\omega_{\text{BH}} := \omega_z|_{r_+}$, to ensure a better convergence [57, 64], and reads $\dot{E}_{\text{BZ}} \simeq (2\pi/3 B_0^2 r_+^2 \omega_{\text{BH}}^2) [1 + 1.38 (M\omega_{\text{BH}})^2 - 9.2 (M\omega_{\text{BH}})^4]$, where, for simplicity, we assumed that the magnetic field at the event horizon is comparable to that at the ergobelt, i.e., $B_{r=r_+}^2 \approx B_0^2 = \sigma_0 w_0$. The bottom part of Fig. 3 reports the ratio $\dot{E}_{\text{rec}}/\dot{E}_{\text{BZ}}$ showing that for sufficiently large BH spins and magnetisations, the plasmoid-driven PP leads to

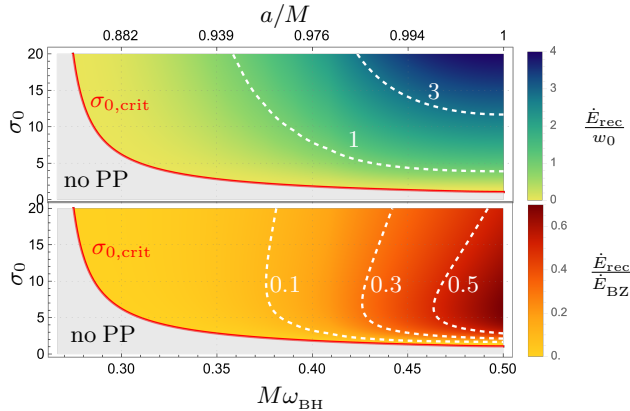


FIG. 3. *Top panel:* Rate of energy extraction per unit of enthalpy density, \dot{E}_{rec}/w_0 , at the ergobelt of a maximally-filling torus as a function of the magnetisation σ_0 and BH angular velocity ω_{BH} (the top horizontal axis uses instead a scale in a/M). The red solid line marks the critical magnetisation $\sigma_{0,\text{crit}}$ below which no PP is possible (grey shaded area). *Bottom panel:* The same as in the top but when the energy extraction rate is normalised to the BZ power $\dot{E}_{\text{rec}}/\dot{E}_{\text{BZ}}$.

an energy extraction that is smaller but comparable to that associated with the BZ mechanism (see also [25, 26] for similar results).

Conclusions. Responding to the increasing evidence that resistive effects in plasmas around BHs play an important role in shaping the observed phenomenology of these objects, we have presented a general approach to the study of a PP driven by plasmoids produced at reconnection sites along current sheets. Our formalism ultimately establishes the physical conditions to make a plasmoid-driven PP energetically viable and can be applied equally to scenarios that are dominated by the plasma or by the magnetic field, that is, in MHD or FFE regimes. It is also genuinely multidimensional and hence allows one to explore conditions that are beyond the ones studied so far and that have been restricted to the equatorial plane. In this sense, it provides a direct contact with numerical simulations, either in MHD [39–43, 45] or with PIC approaches [25, 58–60], all of which highlight an intense reconnection activity outside the equatorial plane. Finally, it does not assume an ad-hoc description of the dynamics of the plasma, or conjecture its kinematic properties with oversimplified and possibly unrealistic configurations. On the contrary, it constructs the dynamics of the plasma starting from a well-known configuration, that of an equilibrium torus with a toroidal magnetic field, and thus possessing all the features necessary to compute self-consistently the reconnection process and estimate the PP energetics.

While the results presented here offer the first coherent approach to a multidimensional treatment of the PP driven by magnetic reconnection, they can be improved in a number of ways. First, by developing a more accurate descriptions of plasmoids that could overcome the limitations of the RAIB model. Second, by exploiting the results of numerical simulations to produce better estimates of the reconnection rate

and hence of the efficiency of the energy-extraction process. Thirdly, by connecting the plasmoid production at the ergobelt with the plasmoid production on the equatorial plane (that remains a favourable site for the production of plasmoids [23–26]), hence join the MHD regime of the plasma in the torus with the FFE regime when the plasma has left the torus and is accreting onto the BH. We plan to investigate these important aspects in future works.

We thank Benoît Cerutti, Luca Comisso, Ileyk El Melah, Claudio Meringolo, Antonios Nathanail, and Kyle Parfrey for insightful discussions and comments. Partial funding comes from the State of Hesse within the Research Cluster ELEMENTS (Project ID 500/10.006), by the ERC Advanced Grant “JETSET: Launching, propagation and emission of relativistic jets from binary mergers and across mass scales” (Grant No. 884631). LR acknowledges the Walter Greiner Gesellschaft zur Förderung der physikalischen Grundlagenforschung e.V. through the Carl W. Fueck Laureatus Chair.

-
- [1] Y. Su, A. M. Veronig, G. D. Holman, B. R. Dennis, T. Wang, M. Temmer, and W. Gan, Imaging coronal magnetic-field reconnection in a solar flare, *Nature Physics* **9**, 489 (2013).
 - [2] E. G. Zweibel and M. Yamada, Magnetic reconnection in astrophysical and laboratory plasmas, *Annual Review of Astronomy and Astrophysics* **47**, 291 (2009).
 - [3] M. Yamada, R. Kulsrud, and H. Ji, Magnetic reconnection, *Rev. Mod. Phys.* **82**, 603 (2010).
 - [4] D. A. Uzdensky and A. Spitkovsky, Physical conditions in the reconnection layer in pulsar magnetospheres, *The Astrophysical Journal* **780**, 3 (2013).
 - [5] A. M. Beloborodov, Radiative magnetic reconnection near accreting black holes, *The Astrophysical Journal* **850**, 141 (2017).
 - [6] B. Ripperda, F. Bacchini, O. Porth, E. R. Most, H. Olivares, A. Nathanail, L. Rezzolla, J. Teunissen, and R. Keppens, General-relativistic Resistive Magnetohydrodynamics with Robust Primitive-variable Recovery for Accretion Disk Simulations, *Astrophys. J., Supp.* **244**, 10 (2019), arXiv:1907.07197 [physics.comp-ph].
 - [7] K. Akiyama and *et al.*, First M87 Event Horizon Telescope Results. V. Physical Origin of the Asymmetric Ring, *Astrophys. J. Lett.* **875**, L5 (2019).
 - [8] Event Horizon Telescope Collaboration, K. Akiyama, *et al.*, First Sagittarius A* Event Horizon Telescope Results. V. Testing Astrophysical Models of the Galactic Center Black Hole, *Astrophys. J. Lett.* **930**, L16 (2022).
 - [9] C. Palenzuela, L. Lehner, O. Reula, and L. Rezzolla, Beyond ideal MHD: towards a more realistic modelling of relativistic astrophysical plasmas, *Mon. Not. R. Astron. Soc.* **394**, 1727 (2009), arXiv:0810.1838.
 - [10] Y. T. Liu, S. L. Shapiro, Z. B. Etienne, and K. Taniguchi, General relativistic simulations of magnetized binary neutron star mergers, *Phys. Rev. D* **78**, 024012 (2008), arXiv:0803.4193 [astro-ph].
 - [11] M. Anderson, E. W. Hirschmann, L. Lehner, S. L. Liebling, P. M. Motl, D. Neilsen, C. Palenzuela, and J. E. Tohline, Magnetized Neutron-Star Mergers and Gravitational-Wave Signals, *Phys. Rev. Lett.* **100**, 191101 (2008), arXiv:0801.4387 [gr-qc].

- [12] L. Rezzolla, B. Giacomazzo, L. Baiotti, J. Granot, C. Kouveliotou, and M. A. Aloy, The Missing Link: Merging Neutron Stars Naturally Produce Jet-like Structures and Can Power Short Gamma-ray Bursts, *Astrophys. J. Letters* **732**, L6 (2011), [arXiv:1101.4298 \[astro-ph.HE\]](#).
- [13] C. Palenzuela, L. Lehner, M. Ponce, S. L. Liebling, M. Anderson, D. Neilsen, and P. Motl, Electromagnetic and Gravitational Outputs from Binary-Neutron-Star Coalescence, *Phys. Rev. Lett.* **111**, 061105 (2013), [arXiv:1301.7074 \[gr-qc\]](#).
- [14] K. Kiuchi, Y. Sekiguchi, K. Kyutoku, M. Shibata, K. Taniguchi, and T. Wada, High resolution magnetohydrodynamic simulation of black hole-neutron star merger: Mass ejection and short gamma ray bursts, *Phys. Rev. D* **92**, 064034 (2015), [arXiv:1506.06811 \[astro-ph.HE\]](#).
- [15] K. Dionysopoulou, D. Alic, and L. Rezzolla, General-relativistic resistive-magnetohydrodynamic simulations of binary neutron stars, *Phys. Rev. D* **92**, 084064 (2015), [arXiv:1502.02021 \[gr-qc\]](#).
- [16] Y.-H. Liu, M. Hesse, F. Guo, W. Daughton, H. Li, P. A. Cassak, and M. A. Shay, Why does steady-state magnetic reconnection have a maximum local rate of order 0.1?, *Phys. Rev. Lett.* **118**, 085101 (2017), [arXiv:1611.07859 \[physics.plasm-ph\]](#).
- [17] L. Comisso and F. A. Asenjo, Thermal-inertial effects on magnetic reconnection in relativistic pair plasmas, *Phys. Rev. Lett.* **113**, 045001 (2014).
- [18] F. Guo, H. Li, W. Daughton, and Y.-H. Liu, Formation of hard power laws in the energetic particle spectra resulting from relativistic magnetic reconnection, *Phys. Rev. Lett.* **113**, 155005 (2014).
- [19] F. A. Asenjo and L. Comisso, Generalized magnetofluid connections in relativistic magnetohydrodynamics, *Phys. Rev. Lett.* **114**, 115003 (2015).
- [20] Y.-H. Liu, F. Guo, W. Daughton, H. Li, and M. Hesse, Scaling of magnetic reconnection in relativistic collisionless pair plasmas, *Phys. Rev. Lett.* **114**, 095002 (2015).
- [21] D. Ball, F. Özel, D. Psaltis, and C.-k. Chan, Particle Acceleration and the Origin of X-Ray Flares in GRMHD Simulations of SGR A, *Astrophys. J.* **826**, 77 (2016), [arXiv:1602.05968 \[astro-ph.HE\]](#).
- [22] C. Meringolo, A. Cruz-Orsorio, L. Rezzolla, and S. Servidio, Microphysical Plasma Relations from Special-relativistic Turbulence, *Astrophys. J.* **944**, 122 (2023), [arXiv:2301.02669 \[astro-ph.HE\]](#).
- [23] S. Koide and K. Arai, Energy Extraction from a Rotating Black Hole by Magnetic Reconnection in Ergosphere, *Astrophys. J.* **682**, 1124 (2008), [arXiv:0805.0044 \[astro-ph\]](#).
- [24] F. A. Asenjo and L. Comisso, Relativistic Magnetic Reconnection in Kerr Spacetime, *Phys. Rev. Lett.* **118**, 055101 (2017), [arXiv:1701.03669 \[astro-ph.HE\]](#).
- [25] K. Parfrey, A. Philippov, and B. Cerutti, First-Principles Plasma Simulations of Black-Hole Jet Launching, *Phys. Rev. Lett.* **122**, 035101 (2019), [arXiv:1810.03613 \[astro-ph.HE\]](#).
- [26] L. Comisso and F. A. Asenjo, Magnetic reconnection as a mechanism for energy extraction from rotating black holes, *Phys. Rev. D* **103**, 023014 (2021).
- [27] A. Bransgrove, B. Ripperda, and A. Philippov, Magnetic Hair and Reconnection in Black Hole Magnetospheres, *Phys. Rev. Lett.* **127**, 055101 (2021), [arXiv:2109.14620 \[astro-ph.HE\]](#).
- [28] J. P. Lasota, E. Gourgoulhon, M. Abramowicz, A. Tchekhovskoy, and R. Narayan, Extracting black-hole rotational energy: The generalized Penrose process, *Phys. Rev. D* **89**, 024041 (2014).
- [29] R. Penrose and R. M. Floyd, Extraction of rotational energy from a black hole, *Nature* **229**, 177 (1971).
- [30] M. Bañados, J. Silk, and S. M. West, Kerr black holes as particle accelerators to arbitrarily high energy, *Phys. Rev. Lett.* **103**, 111102 (2009).
- [31] M. Bejger, T. Piran, M. Abramowicz, and F. Håkanson, Collisional Penrose Process near the Horizon of Extreme Kerr Black Holes, *Phys. Rev. Lett.* **109**, 121101 (2012), [arXiv:1205.4350 \[astro-ph.HE\]](#).
- [32] J. D. Schnittman, Revised upper limit to energy extraction from a Kerr black hole, *Phys. Rev. Lett.* **113**, 261102 (2014).
- [33] E. Berti, R. Brito, and V. Cardoso, Ultrahigh-Energy Debris from the Collisional Penrose Process, *Phys. Rev. Lett.* **114**, 251103 (2015), [arXiv:1410.8534 \[gr-qc\]](#).
- [34] W. H. Press and S. A. Teukolsky, Floating Orbits, Superradiant Scattering and the Black-hole Bomb, *Nature* **238**, 211 (1972).
- [35] P. Pani, V. Cardoso, L. Gualtieri, E. Berti, and A. Ishibashi, Black-hole bombs and photon-mass bounds, *Phys. Rev. Lett.* **109**, 131102 (2012).
- [36] P. Bosch, S. R. Green, and L. Lehner, Nonlinear evolution and final fate of charged anti-de Sitter black hole superradiant instability, *Phys. Rev. Lett.* **116**, 141102 (2016).
- [37] W. E. East and F. Pretorius, Superradiant instability and back-reaction of massive vector fields around Kerr black holes, *Phys. Rev. Lett.* **119**, 041101 (2017).
- [38] R. D. Blandford and R. L. Znajek, Electromagnetic extractions of energy from Kerr black holes, *Mon. Not. Roy. Astron. Soc.* **179**, 433 (1977).
- [39] J. F. Mählmann, A. Levinson, and M. A. Aloy, Striped Blandford/Znajek jets from advection of small-scale magnetic field, *Mon. Not. R. Astron. Soc.* **494**, 4203 (2020), [arXiv:2001.03171 \[astro-ph.HE\]](#).
- [40] B. Ripperda, F. Bacchini, and A. A. Philippov, Magnetic Reconnection and Hot Spot Formation in Black Hole Accretion Disks, *Astrophys. J.* **900**, 100 (2020), [arXiv:2003.04330 \[astro-ph.HE\]](#).
- [41] A. Nathanail, C. M. Fromm, O. Porth, H. Olivares, Z. Younsi, Y. Mizuno, and L. Rezzolla, Plasmoid formation in global GRMHD simulations and AGN flares, *Mon. Not. R. Astron. Soc.* **495**, 1549 (2020), [arXiv:2002.01777 \[astro-ph.HE\]](#).
- [42] A. Nathanail, R. Gill, O. Porth, C. M. Fromm, and L. Rezzolla, 3D magnetized jet break-out from neutron-star binary merger ejecta: afterglow emission from the jet and the ejecta, *Mon. Not. R. Astron. Soc.* **502**, 1843 (2021), [arXiv:2009.09714 \[astro-ph.HE\]](#).
- [43] B. Ripperda, M. Liska, K. Chatterjee, G. Musoke, A. A. Philippov, S. B. Markoff, A. Tchekhovskoy, and Z. Younsi, Black Hole Flares: Ejection of Accreted Magnetic Flux through 3D Plasmoid-mediated Reconnection, *Astrophys. J. Lett.* **924**, L32 (2022), [arXiv:2109.15115 \[astro-ph.HE\]](#).
- [44] B. Crinquant, B. Cerutti, G. Dubus, K. Parfrey, and A. Philippov, Synthetic images of magnetospheric reconnection-powered radiation around supermassive black holes, *Phys. Rev. Lett.* **129**, 205101 (2022).
- [45] I. Dimitropoulos, A. Nathanail, M. Petropoulou, and I. Contopoulos, Flares from plasmoids and current sheets around Sgr A*, *preprint* (2024), [arXiv:2407.14312 \[astro-ph.HE\]](#).
- [46] L. Rezzolla and O. Zanotti, *Relativistic Hydrodynamics* (Oxford University Press, 2013).
- [47] S. E. Gralla and T. Jacobson, Spacetime approach to force-free magnetospheres, *Mon. Not. Roy. Astron. Soc.* **445**, 2500 (2014), [arXiv:1401.6159 \[astro-ph.HE\]](#).
- [48] J. C. McKinney, General relativistic force-free electrodynamics: a new code and applications to black hole magnetospheres, *Mon. Not. Roy. Astron. Soc.* **367**, 1797 (2006), [arXiv:astro-ph/0601410](#).

- [49] A. Chael, A. Lupsasca, G. N. Wong, and E. Quataert, Black Hole Polarimetry I. A Signature of Electromagnetic Energy Extraction, *Astrophys. J.* **958**, 65 (2023), arXiv:2307.06372 [astro-ph.HE].
- [50] S. S. Komissarov, Electrodynamics of black hole magnetospheres, *Mon. Not. R. Astron. Soc.* **350**, 427 (2004), arXiv:astro-ph/0402403.
- [51] Z. Gelles, A. Chael, and E. Quataert, Signatures of Black Hole Spin and Plasma Acceleration in Jet Polarimetry, preprint (2024), arXiv:2410.00954 [astro-ph.HE].
- [52] S. S. Komissarov, Magnetized tori around Kerr black holes: analytic solutions with a toroidal magnetic field, *Mon. Not. R. Astron. Soc.* **368**, 993 (2006), astro-ph/0601678.
- [53] P. J. Montero, O. Zanotti, J. A. Font, and L. Rezzolla, Dynamics of magnetized relativistic tori oscillating around black holes, *Mon. Not. R. Astron. Soc.* **378**, 1101 (2007), arXiv:astro-ph/0702485.
- [54] S. Gimeno-Soler and J. A. Font, Magnetised Polish doughnuts revisited, *Astron. Astrophys.* **607**, A68 (2017).
- [55] D. A. Uzdensky, Force-Free Magnetosphere of an Accretion Disk-Black Hole System. II. Kerr Geometry, *Astrophys. J.* **620**, 889 (2005), arXiv:astro-ph/0410715.
- [56] A. Nathanail and I. Contopoulos, Black Hole Magnetospheres, *Astrophys. J.* **788**, 186 (2014), arXiv:1404.0549 [astro-ph.HE].
- [57] F. Camilloni, O. J. C. Dias, G. Grignani, T. Harmark, R. Olivieri, M. Orselli, A. Placidi, and J. E. Santos, Blandford-Znajek monopole expansion revisited: novel non-analytic contributions to the power emission, *JCAP* **07** (07), 032, arXiv:2201.11068 [gr-qc].
- [58] I. El Mellah, B. Cerutti, B. Crinquand, and K. Parfrey, Spinning black holes magnetically connected to a Keplerian disk - Magnetosphere, reconnection sheet, particle acceleration, and coronal heating, *Astron. Astrophys.* **663**, A169 (2022), arXiv:2112.03933 [astro-ph.HE].
- [59] I. El Mellah, B. Cerutti, and B. Crinquand, Reconnection-driven flares in 3D black hole magnetospheres - A scenario for hot spots around Sagittarius A*, *Astron. Astrophys.* **677**, A67 (2023), arXiv:2305.01689 [astro-ph.HE].
- [60] J. Vos, B. Cerutti, M. Moscibrodzka, and K. Parfrey, Particle Acceleration in Collisionless Magnetically Arrested Disks, preprint (2024), arXiv:2410.19061 [astro-ph.HE].
- [61] Y. E. Lyubarsky, On the relativistic magnetic reconnection, *Mon. Not. Roy. Astr. Soc.* **358**, 113 (2005), arXiv:astro-ph/0501392.
- [62] P. A. Cassak, Y. H. Liu, and M. A. Shay, A Review of the 0.1 Reconnection Rate Problem, *J. Plasma Phys.* **83**, 715830501 (2017), arXiv:1708.03449 [physics.plasm-ph].
- [63] Y.-M. Huang and A. Bhattacharjee, Distribution of plasmoids in high-lundquist-number magnetic reconnection, *Phys. Rev. Lett.* **109**, 265002 (2012).
- [64] A. Tchekhovskoy, R. Narayan, and J. C. McKinney, Black Hole Spin and the Radio Loud/Quiet Dichotomy of Active Galactic Nuclei, *Astrophys. J.* **711**, 50 (2010), arXiv:0911.2228 [astro-ph.HE].
- [65] M. Abramowicz, M. Jaroszynski, and M. Sikora, Relativistic, accreting disks, *Astron. Astrophys.* **63**, 221 (1978).
- [66] M. Kozłowski, M. Jaroszynski, and M. A. Abramowicz, The analytic theory of fluid disks orbiting the Kerr black hole, *Astron. and Astrophys.* **63**, 209 (1978).

End Matter

In what follows we provide the most important details about the calculations or considerations that are needed to obtain the results presented in the main text.

Kerr metric and ZAMO frame. The Kerr metric in Boyer-Lindquist (BL) coordinates $x^\mu = (t, r, \theta, \phi)$ and in a (3 + 1)-form reads $ds^2 = g_{\mu\nu} dx^\mu dx^\nu = -\alpha^2 dt^2 + \gamma_{ij} (dx^i + \beta^i dt)(dx^j + \beta^j dt)$ with the lapse function, the shift vector and the absolute space metric respectively defined as

$$\alpha = \frac{1}{\sqrt{-g^{tt}}} = \sqrt{\Delta\Sigma/\Pi}, \quad \beta^i = \alpha^2 g^{ti} = -\alpha^2 a r r_0 / \Delta \Sigma, \quad (5)$$

$$\gamma_{ij} dx^i dx^j = \Sigma/\Delta dr^2 + \Sigma d\theta^2 + \Pi/\Sigma \sin^2 \theta d\phi^2, \quad (6)$$

and the metric determinant decomposes as $g = -\alpha^2 \det(\gamma_{ij})$. The metric functions explicitly read $\Delta = r^2 - 2Mr + a^2$, $\Sigma = r^2 + a^2 \cos^2 \theta$ and $\Pi = (r^2 + a^2)^2 - a^2 \Delta \sin^2 \theta$, with the event horizon position given by the r_+ root of $\Delta = (r - r_+)(r - r_-)$, $r_\pm = M(1 \pm \sqrt{1 - a_*^2})$, and the ergosphere location at $r_0(\theta) = M(1 + \sqrt{1 - a_*^2 \cos^2 \theta})$, where $a_* := a/M$. We assume the BH to have $0 \leq a_* \leq 1$, with the upper bound imposed by the cosmic censorship conjecture. Other interesting locations in the BH equatorial plane, $\theta = \pi/2$, are given by the marginally stable corotating (+) and counterrotating (-) circular orbit, $r_{\text{ms},\pm}$, and by the marginally bound circular orbit $r_{\text{ms},\pm}$.

The ZAMO is a normal observer (the corresponding 1-form in BL coordinates is $\eta = -\alpha dt$), with an associated local Cartesian right-handed frame $\hat{e}_{(\alpha)} = (\hat{e}_{(T)}, \hat{e}_{(X)}, \hat{e}_{(Y)}, \hat{e}_{(Z)})$ specified by the vectors $\hat{e}_{(T)} = \eta$, $\hat{e}_{(X)} = \partial_r / \sqrt{\gamma_{rr}}$, $\hat{e}_{(Y)} = \partial_\phi / \sqrt{\gamma_{\phi\phi}}$ and $\hat{e}_{(Z)} = -\partial_\theta / \sqrt{\gamma_{\theta\theta}}$, and form a tetrad, namely, $g_{\mu\nu} = \hat{e}_\mu^{(\alpha)} \hat{e}_\nu^{(\beta)} \hat{\eta}_{(\alpha)(\beta)}$ and $\varepsilon_{\mu\nu\rho\sigma} = \hat{e}_\mu^{(T)} \wedge \hat{e}_\nu^{(X)} \wedge \hat{e}_\rho^{(Y)} \wedge \hat{e}_\sigma^{(Z)}$, where $\hat{\eta}_{(\alpha)(\beta)}$ is the Minkowski metric in the local frame and $\varepsilon_{\mu\nu\rho\sigma} := \sqrt{-g} \eta_{\mu\nu\rho\sigma}$ is the 4-dimensional Levi-Civita tensor.

Plasma velocity. As mentioned in the main text, the character of the field is set by the invariant quantity $F^{\mu\nu} F_{\mu\nu} = 2(\mathcal{B}^2 - \mathcal{E}^2)$, with the strength of the ZAMO fields given by

$$\mathcal{B}^2 = \frac{1}{\sin^2 \theta} \left[\frac{\Delta(\partial_r \Psi)^2 + (\partial_\theta \Psi)^2}{\Pi} + \frac{I^2}{\Delta} \right], \quad (7)$$

$$\mathcal{E}^2 = \mathcal{F}^2(\Omega) \frac{\Delta(\partial_r \Psi)^2 + (\partial_\theta \Psi)^2}{\Pi \sin^2 \theta},$$

and where we introduced $\mathcal{F}(\Omega) := \sqrt{\gamma_{\phi\phi}}(\omega_z - \Omega)/\alpha$. Notice that $\mathcal{F}(\Omega) = \pm 1$ at the outer/inner light surfaces, i.e., the locations where corotating observers with the field lines become null, $|\partial_t + \Omega(\Psi)\partial_\phi|^2 = \alpha^2(\mathcal{F}^2(\Omega) - 1) = 0$, or equivalently, where the magnetic field transitions from being dominated by poloidal to toroidal components.

The orthonormal vectors (see Eq. (1) in the main text), valid for degenerate fields, are conveniently parameterised in terms of two magnetic orientation angles $\xi_1 := \tan^{-1}(\hat{\mathcal{B}}^{(Y)}/\hat{\mathcal{B}}^{(X)})$

and $\xi_2 := \cos^{-1}(\hat{\mathcal{B}}^{(Z)}/\sqrt{\mathcal{B}^2})$ with respect to the ZAMO frame, such that

$$\begin{aligned} \sin \xi_1 &= -\sqrt{\Pi I}/\sqrt{\Delta(\partial_\theta \Psi)^2 + \Pi I^2}, \\ \sin \xi_2 &= \sqrt{(\Pi I^2 + \Delta(\partial_\theta \Psi)^2)/(\Pi I^2 + \Delta(\Delta(\partial_r \Psi)^2 + (\partial_\theta \Psi)^2))}, \end{aligned} \quad (8)$$

$$\begin{aligned} \mathcal{X} &= \mathcal{X}^{(\alpha)} \hat{e}_{(\alpha)} = (\cos \xi_2/\chi) \hat{e}_{(X)} - (\cos \xi_1 \sin \xi_2/\chi) \hat{e}_{(Z)} \\ \mathcal{Y} &= \mathcal{Y}^{(\alpha)} \hat{e}_{(\alpha)} = \cos \xi_1 \sin \xi_2 \hat{e}_{(X)} + \sin \xi_1 \sin \xi_2 \hat{e}_{(Y)} + \cos \xi_2 \hat{e}_{(Z)}, \\ \mathcal{Z} &= \mathcal{Z}^{(\alpha)} \hat{e}_{(\alpha)} = -(\cos \xi_1 \sin \xi_1 \sin^2 \xi_2/\chi) \hat{e}_{(X)} + \chi \hat{e}_{(Y)} - (\cos \xi_2 \sin \xi_1 \sin \xi_2/\chi) \hat{e}_{(Z)}, \end{aligned} \quad (9)$$

where $\chi := \sqrt{1 - (\sin \xi_1 \sin \xi_2)^2}$.

As anticipated in the main text, it is possible to use such a set of vectors to construct the most general four-velocity that is compatible with the electric-field screening condition. More specifically, the velocity perpendicular to the fields can be written as $\hat{v}_\perp^2 = \mathcal{F}^2(\Omega)(1 - \hat{\mathcal{B}}_{(Y)}^2/\mathcal{B}^2)$. The parallel component, instead, can be parametrized as $\hat{v}_\parallel := q \hat{v}_\parallel^{\max} = q/\hat{\gamma}$ with $q \in (-1, 1)$ and $\hat{\gamma} = \hat{\gamma}_\perp/\sqrt{1 - q^2}$. In the ZAMO Cartesian frame, the components of the spatial velocity read

$$\hat{v}^{(X)} = \left(\mathcal{F} \frac{\hat{\mathcal{B}}^{(Y)}}{\mathcal{B}} + q \sqrt{1 - \mathcal{F}^2 \left(1 - \frac{\hat{\mathcal{B}}_{(Y)}^2}{\mathcal{B}^2} \right)} \right) \frac{\hat{\mathcal{B}}^{(X)}}{\mathcal{B}}, \quad (10)$$

$$\hat{v}^{(Y)} = \mathcal{F} \left(\frac{\hat{\mathcal{B}}_{(Y)}^2}{\mathcal{B}^2} - 1 \right) + q \sqrt{1 - \mathcal{F}^2 \left(1 - \frac{\hat{\mathcal{B}}_{(Y)}^2}{\mathcal{B}^2} \right)} \frac{\hat{\mathcal{B}}^{(Y)}}{\mathcal{B}}, \quad (11)$$

$$\hat{v}^{(Z)} = \left(\mathcal{F} \frac{\hat{\mathcal{B}}^{(Y)}}{\mathcal{B}} + q \sqrt{1 - \mathcal{F}^2 \left(1 - \frac{\hat{\mathcal{B}}_{(Y)}^2}{\mathcal{B}^2} \right)} \right) \frac{\hat{\mathcal{B}}^{(Z)}}{\mathcal{B}}, \quad (12)$$

where $0 \leq q \leq 1$ is a free coefficients and where the expressions above reduce to the previous results in the literature under the appropriate limits³ Furthermore, it is easy to verify that the components (10) and (12) satisfy the standard relation $\hat{v}^{(X)}/\hat{\mathcal{B}}^{(X)} = \hat{v}^{(Z)}/\hat{\mathcal{B}}^{(Z)}$.

On the magnetised torus. Equations (10)–(12) show that if the magnetic field is purely toroidal, $\hat{\mathcal{B}} = \hat{\mathcal{B}}^{(Y)} \hat{e}_{(Y)}$, the same is true for the plasma velocity $\hat{v} = q \hat{e}_{(Y)}$, so that the velocity is purely parallel to the field lines. This is the basic dynamical property of the plasma in a Komissarov torus. Furthermore, the condition for the four-velocity to be that of a circular motion with angular velocity Ω_0 as seen by an asymptotic observer requires that $\hat{v}_\parallel = q = \mathcal{F}(\Omega_0)$. We here are interested in tori with a constant specific angular-momentum

with explicit expressions given by

$\ell_0 := u_\phi/u_t$ and corotating with the BH ($\ell_0 = \text{const.} > 0$), so that the magnetic field is aligned with the azimuthal coordinate, i.e., $\Psi = 0$ and $I < 0$, so that $\xi_{1,2} = \pi/2$ [see Eq. (8)]. In this case, $\Omega_0 := -(g_{t\phi} + g_{tt}\ell_0)/(g_{\phi\phi} + g_{t\phi}\ell_0)$, and we can express the parallel velocity as a function of ℓ_0 as $\hat{v}_\parallel = \alpha \ell_0 / [\sqrt{\gamma_{\phi\phi}}(\omega_z \ell_0 - 1)]$. With these assumptions, together with the condition $\tilde{v}_{\text{out}} \approx \sqrt{\sigma_0/(1 + \sigma_0)}$ and $\tilde{\gamma}_{\text{out}} \approx \sqrt{1 + \sigma_0}$ [16], Eq. (3) reduces to

$$\begin{aligned} \varepsilon_\pm^\infty &= \alpha \hat{\gamma} \left[\left(1 + \frac{\sqrt{\gamma_{\phi\phi}} \omega_z \hat{v}_\parallel}{\alpha} \right) \sqrt{1 + \sigma_0} \right. \\ &\quad \left. \pm \left(\hat{v}_\parallel + \frac{\sqrt{\gamma_{\phi\phi}} \omega_z}{\alpha} \right) \sqrt{\sigma_0} - \frac{1}{4} \frac{\sqrt{1 + \sigma_0} - \hat{v}_\parallel \sqrt{\sigma_0}}{\hat{\gamma}^2 (1 + \sigma_0 - \hat{v}_\parallel^2 \sigma_0)} \right]. \end{aligned} \quad (13)$$

We should note that although we derive Eq. (13) as a limit of Eq. (3) for $\hat{v}_\parallel = \alpha \ell_0 / [\sqrt{\gamma_{\phi\phi}}(\omega_z \ell_0 - 1)]$ and $\tilde{v}_{\text{out}} \approx \sqrt{\sigma_0/(1 + \sigma_0)}$, it coincides with Eq. (34) in Ref. [26], where the plasma was assumed to be in a Keplerian circular orbit in the equatorial plane. Within these limits, therefore, Eq. (34) in [26] would provide a multidimensional expression for the plasmoid energies when the Keplerian velocity is replaced by a generic nonplanar one.

We notice that the comoving magnetic field satisfies $b^t = \ell_0 b^\phi$, as typical in the Komissarov torus [50], with $b^t = -\hat{v}_\parallel \hat{\gamma}_\parallel \hat{\mathcal{B}}^{(Y)}/\alpha^4$. The torus is traditionally defined by equipotential surfaces specified by the condition [65, 66]

$$\mathcal{W} = \frac{1}{2} \ln \left| \frac{\alpha^2 \gamma_{\phi\phi}}{\gamma_{\phi\phi} (1 - \ell_0 \omega_z)^2 - \alpha^2 \ell_0^2} \right| = \text{const.} \quad (14)$$

We label with $\mathcal{W}_{\text{cusp}}$ the equipotential surface intersecting the equatorial plane at the corresponding cusp radius r_{cusp} , for which the angular momentum matches the Keplerian value $\ell_0 = \ell_K$, and whose value is solely specified in terms of ℓ_0 and a , whereas \mathcal{W}_{in} labels the torus inner edge, that must be specified as a boundary condition. Furthermore, a choice for

³ For $q = 0$, expressions (10)–(12) coincide with (D140) in Ref. [49], and for $q = 1$ with (A12) in Ref. [50]. Furthermore, the following relations hold: $\hat{\mathcal{B}}^{(X)} = \sqrt{\gamma_{rr}} \hat{\mathcal{B}}^r$, $\hat{\mathcal{B}}^{(Y)} = \sqrt{\gamma_{\phi\phi}} \hat{\mathcal{B}}^\phi$ and $\hat{\mathcal{B}}^{(Z)} = -\sqrt{\gamma_{\theta\theta}} \hat{\mathcal{B}}^\theta$.

⁴ In the notation used in Ref. [50], $b^\phi = \pm \sqrt{2p_m/\mathcal{A}}$, where $p_m := b^2/2 = \hat{\mathcal{B}}_{(Y)}^2/2$ and $\mathcal{A} := g_{\phi\phi} + 2\ell_0 g_{t\phi} + \ell_0^2 g_{tt} = \alpha^2 \ell_0^2 (1 - \hat{v}_\parallel^2)/\hat{v}_\parallel^2$.

ℓ_0 uniquely determines the locations of the cusp and of the position of the (pressure) rest-mass density maximum and is constrained to be $\ell_0 > \ell_{\text{ms}}$ [46]. If $\ell_{\text{ms}} \leq \ell_0 \leq \ell_{\text{mb}}$, then $\mathcal{W}_{\text{cusp}}$ is guaranteed to be non-positive, so that matter and fields can fill the torus up to the cusp, $\mathcal{W}_{\text{in}} \leq \mathcal{W}_{\text{cusp}}$. In the limiting case $\ell_0 = \ell_{\text{mb}}$, the outermost equipotential surface is marginally closed, i.e., $\mathcal{W}_{\text{cusp}} = 0$, while if $\mathcal{W}_{\text{in}} = 0$ the torus is said to be maximally filled. Conversely, if $\ell_0 > \ell_{\text{mb}}$, then $\mathcal{W}_{\text{cusp}} > 0$, and matter never reaches the cusp being confined within the regions where $\mathcal{W}_{\text{in}} < 0$. In our construction, we always consider tori that are maximally filled, $\mathcal{W}_{\text{in}} = \mathcal{W}_{\text{cusp}} = 0$, since this arguably represents the most interesting configuration, with the torus configuration fully specified by the BH spin and with matter at the cusp prone to accrete onto the BH if perturbed.

The area of the ergobelt is determined by an implicit equation $\mathcal{W}_{\text{in}}(r, \theta) = \mathcal{W}_0$. Because of the non-trivial location of the ergobelt, the surface differential dA is given by $dA = \sqrt{\gamma_{\phi\phi}d\phi^2 \sqrt{\gamma_{\theta\theta}d\theta^2 + \gamma_{rr}dr^2}} \Big|_{\mathcal{W}_0}$, with $\phi \in [0, 2\pi]$ and $\theta \in [\theta_*, \pi/2]$, where θ_* is the polar angle that limits the effective region from above at given σ_0 , ℓ_0 and a . The minimum value θ_*^{m} (i.e., the maximum of the integral support, corresponding to the optimal condition $\sigma_0 \gg 1$) can be determined analytically by inverting Eq. (14) with the supplementary condition $r = r_0(\theta_*^{\text{m}})$, so that

$$\cos(2\theta_*^{\text{m}}) = 1 + 4f_0\ell_0/[a_*M(1-2f_0)] + 4f_0/[a_*^2(1-2f_0)^2] \left(f_0 - 1 + \sqrt{(f_0-1)^2 - a_*^2(1-2f_0)^2 + 2a_*\ell_0f_0(2f_0-1)/M} \right), \quad (15)$$

where $f_0 := e^{2\mathcal{W}_0}$. For a maximally filled torus, $f_0 = 1$, and $\cos(2\theta_*^{\text{m}}) = 1 - 4\ell_0/a + 4M\sqrt{2\ell_0 - a}/a^{3/2}$, which consistently leads to $\theta_*^{\text{m}} = \pi/2$ for $a_{\text{crit}} = 2(\sqrt{2} - 1)M$.

Relativistic Adiabatic Incompressible Balls (RAIBs). In what follows we recall the calculation of the energy-at-infinity of a RAIB starting from the energy momentum tensor of an ideal fluid, following the original discussion of Koide and Arai [23]. The hydrodynamic energy and angular momentum as measured by a ZAMO can be obtained by projecting the fluid part of the energy-momentum tensor $T_{\text{fl}}^{\mu\nu}$ (i.e., not containing electromagnetic contributions) over the ZAMO tetrad

$$\hat{e}_{\text{fl}} := T_{\text{fl}}^{(T)(T)} = -p + w\hat{\gamma}^2, \quad \hat{\ell}_{\text{fl}} := T_{\text{fl}}^{(T)(Y)} = w\hat{\gamma}^2\hat{v}^{(Y)}, \quad (16)$$

where $T_{\text{fl}}^{\mu\nu} := wu^\mu u^\nu + pg^{\mu\nu}$, with w and p the enthalpy density and the pressure measured in the comoving frame of the fluid, and $\hat{\gamma}$ the Lorentz factor of the fluid with respect to the ZAMO. The conserved Noether currents in stationary and axisymmetric hydrodynamic flows, $\mathcal{J}_E^\mu = -T^\mu{}_\nu(\partial_t)^\nu$ and $\mathcal{J}_L^\mu = T^\mu{}_\nu(\partial_\phi)^\nu$, can be expressed as combinations of quantities measured in the ZAMO frame, with their redshifted temporal components being respectively the energy density and angular momentum at infinity, respectively $e^\infty = \alpha\hat{e} + \sqrt{\gamma_{\phi\phi}}\omega_z\hat{\ell}$, and $\ell^\infty = \sqrt{\gamma_{\phi\phi}}\hat{\ell}$.

Assuming the fluid to be perfect and described by an ideal-fluid equation of state, the pressure can be expressed as $p =$

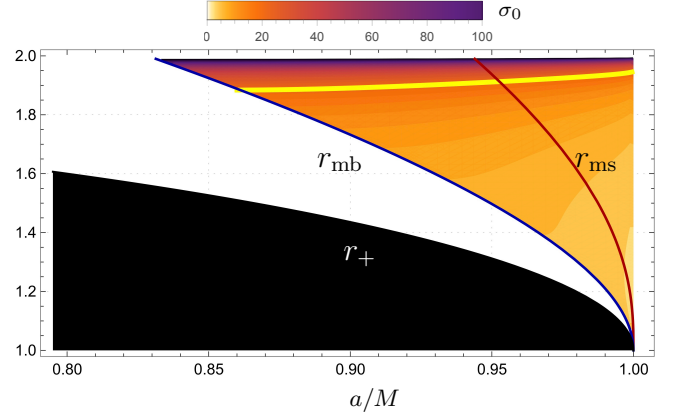


FIG. 4. The same as Fig. 2 but for $\theta = \pi/2$ and illustrating the (r, a) -dependence. For each BH spin, the torus cusp is located between r_{mb} (black line) and r_{ms} (red line). Maximally filled tori penetrate the ergosphere ($r_0 = 2M$ on the equator) for $a/M \gtrsim 0.83$. Tori with the cusp at the largest possible position ($r_{\text{cusp}} = r_{\text{ms}}$ or $\ell_0 = \ell_{\text{ms}}$) require larger BH spins, $a/M \gtrsim 0.94$. By increasing the BH spin $r_{\text{ms}} \rightarrow r_{\text{mb}} \rightarrow r_+$, the ergobelt area grows and comparatively smaller magnetisations are needed for a plasmoid-mediated PP.

$\rho\epsilon(\Gamma - 1)$, with Γ the adiabatic index, ρ the rest-mass density, and ϵ the specific internal energy. As a result, the enthalpy density is $w = \rho(1 + \epsilon\Gamma) = \rho + 4p$ for a completely degenerate relativistic electron fluid with $\Gamma = 4/3$ [46]. For simplicity, we assume that the rest-mass density of the plasmoid is much smaller than the internal energy density, i.e., $\rho \ll \rho\epsilon$, so that the enthalpy density can be approximated as $w = \rho + 4p \approx 4p$. Future improvement to the approach followed here (and in the literature) will concentrate on better estimating not only the role of the rest-mass density over the internal energy density, but also on the role played by the magnetisation in the plasma.

Bearing these considerations in mind, we recall that the RAIB model assumes that the rest-mass density is localised, so that, in the ZAMO frame, $\rho = m\delta^3(\hat{x} - \hat{x}(t))/\hat{\gamma}(t)$, where m is the rest-mass of the RAIB. This allows to easily integrate the energy and angular momentum density over the entire three-space in the ZAMO frame to obtain the total energy and angular momentum at infinity associated to a RAIB

$$E_{\text{RAIB}}^\infty = \alpha \left[H\hat{\gamma} \left(1 + \frac{\sqrt{\gamma_{\phi\phi}}\omega_z\hat{v}^{(y)}}{\alpha} \right) - \frac{U(\Gamma - 1)}{\hat{\gamma}} \right], \quad (17)$$

$$L_{\text{RAIB}}^\infty = \sqrt{\gamma_{\phi\phi}} H\hat{\gamma}\hat{v}^{(Y)}. \quad (18)$$

In obtaining the expressions above we have written the total enthalpy as $H = m(1 + \epsilon\Gamma)$ and the total internal energy as $U = m\epsilon$ [Eq. (17) coincides with Eq. (3) in the main text].

We conclude this section by clarifying an inconsistency often encountered in the literature that adopts the RAIB prescription. It should be noted that in Ref. [26] [see Eq. (25) therein], and in many related works, the expression above is improperly identified as an energy density. The inconsistency becomes evident once realised that if Eq. (25) in [26] corresponds to an energy density, it can be further integrated in space to obtain the total energy, and upon taking the point-

like particle limit (i.e., $U = 0$ and $H = m$) in flat spacetime ($\alpha = 1$ and $\omega_z = 0$), this would lead to $E = m$. Conversely,

the point-like particle limit in flat spacetime of Eq. (3) leads to the correct result for the total relativistic energy of a single particle, i.e., $E = m\hat{\gamma}$.